PREPRINT UCRL-78466

CONF-760859--3

Lawrence Livermore Laboratory

FLASH X-RAY

Quintin Johnson and Donald Pellinen

September 7, 1976

This paper was prepared for the 23rd Sagamore Conference, August 24-27, 1976, Raquette Lake, New York.

FLASH X-RAY

QUINTIN JOHNSON*
Lawrence Livermore Laboratory, University of California
Livermore, California 94550
and
DONALD PELLINEN
Physics International
2700 Merced Street
San Leandro, California 94577

ABSTRACT

The complementary techniques of flash x-ray radiography (FXR) and flash x-ray diffraction (FXD) provide access to a unique domain in nondestructive materials testing. FXR is useful in studies of *macro*scopic properties during extremely short time intervals, and FXD, the newer technique, is used in studies of *micro*scopic properties. Although these techniques are similar in many respects, there are some substantial differences. FXD generally requires low-voltage, line-radiation sources and extremely accurate timing; FXR is usually less demanding. Phenomena which can be profitably studied by FXR often can also be studied by FXD to permit a complete materials characterization.

INTRODUCTION

Flash X-ray (FX) is a borderline nondestructive testing (NDT) technique. Although X-rays are, for the most part, nondestructive, the fact that FX methods require less than one μs per exposure makes them ideally suited to the task of probing material that is moving or changing very rapidly, and the acceleration or deceleration necessarily involved in such tests often destroys

*Work performed under the auspices of the U. S. Energy Research and Development Administration under contract No. W-7405-Eng-48.

the material. FX can thus be viewed as a NDT technique for materials on their way to being destroyed!

Flash x-ray radiography (FXR) is nothing more than the x-ray equivalent of optical strobing. It is used to probe the inside of fast-moving objects and to examine detail in cases where object self-illumination presents a problem. Often, such events cannot be viewed by other techniques. FXR is especially valuable in revealing *macro*scopic changes in volume or density. A typical system will use a pulse 10^{-8} to 10^{-7} s in length. The blur will be equal to the product of the object velocity and the exposure time. For example, if a bullet from a 220 Swift, which has a muzzle velocity of 1.2 km/s, were radiographed with a relatively slow 10^{-7}-s pulse system, the motion blur would be only 1.2×10^{-2} cm. FXR can be used to define accurately the bullet's location as it moves through opaque media (the barrel, the muzzle brake, or the target).

Flash x-ray diffraction (FXD) is a more recent development which makes use of coherent elastic scattering. It is sensitive to *micro*scopic changes (simple atomic displacements or complete rearrangements as in a crystalline structure transformation).

Combining these two techniques makes it possible to access a unique domain in NDT. The type of phenomena observable by the two FX methods and the exposure times required are shown in Fig. 1. Exposure times for some continuous x-ray studies are also shown. Most of the short-lived phenomena have already been explored in some detail. One exception, however, is the interaction of lasers with various materials. It is anticipated that as shorter pulse machines and techniques become available, studies of laser phenomena will begin.

ELEMENTS OF A FLASH X-RAY EXPERIMENT

ENERGY STORAGE, PULSE SHAPING

As shown in Fig. 2, FX experiments typically involve seven basic elements in addition to the power supply. The first of these is the energy storage unit. (The others will be discussed in turn.) The simplest and most common way to store energy is in a low-inductance capacitor. If this energy-storage unit is connected directly to an evacuated x-ray tube, as shown in Fig. 3, a simple FX device results. Charging the capacitor C through the isolation resistor R leads ultimately to a flash discharge in the x-ray tube resulting in a pulse of X-rays. (It is assumed that the circuit is completed by connection of the left- and right-hand parts of the circuit and that the anode/cathode gap in the x-ray tube is small enough to break down before the capacitor does.) This is not a very sophisticated system; it lacks provision for both timing and pulse shaping. The incorporation of a simple triggered spark gap (shown in the lower left-hand side) corrects the first of these deficiencies. The right-hand circuit component, a spark gap and pulse transformer, addresses both.

A more sophisticated approach is shown in Fig. 4. This is a schematic drawing of a Marx generator [2], which combines energy-storage and pulse-shaping functions in a deceptively simple circuit. Such generators allow one to charge the capacitors in parallel and to discharge them in series. This permits erection of a fast, high-voltage pulse from relatively simple circuit components. After the capacitors are charged to a suitable voltage, discharge is initiated through the triggered spark gap shown on the left. In simple Marx systems, the following gap then breaks down as a result of an over-voltage transient. The avalanche thus started leads to a fast-rising voltage

pulse on the x-ray tube equal to and in some cases greater than the charging potential times the number of stages. In more complicated hybrid triggering systems, a number of gaps are triggered, and the remainder are capacitively coupled to ensure fast erection with low jitter [3].

Rather large Marx generator arrays are used to produce the very high voltages required for state-of-the-art FX devices. An example is the array used in a recently fabricated 9-MeV device [4] and shown in Fig. 5. In the photograph, it is possible to see individual capacitors, connecting spark gaps, and clear plastic tubes filled with a $CuSO_4$ solution, which function as the isolation resistors. In operation, the whole room is filled with oil to prevent high voltage breakdown. The complete x-ray device is shown in Fig. 6. The box-shaped unit at the upper right of the figure is the tank containing the Marx generator. This is connected to a cylindrical unit containing a Blumlein pulse transformer. The actual electron-accelerator x-ray head is at the lower left.

At the other end of the scale of complexity from the 9-MeV device described above is the Blumlein FX device used in FXD studies at the Lawrence Livermore Laboratory (LLL). Shown schematically in Fig. 7, it combines energy-storage and pulse-forming components. Basically, it consists of a low-impedance, triaxial transmission line approximately 20 cm in diameter and 7 m long. The indicated conductor is charged by a power supply to 50 to 60 keV. To initiate a discharge, this conductor is connected to the outer conductor via a triggered spark gap. The Blumlein circuit employed in this FX unit enables a voltage gain on the x-ray head over the charging value according to the following:

$$V/V_0 = 2Z_1/(Z_0 + Z_1), \qquad (1)$$

where Z_l is the load (anode/cathode-gap) impedance and Z_0 is the characteristic impedance of the Blumlein [5]. Since it is desirable to keep the voltage relatively low while increasing the electron current to enhance the component of characteristic radiation [6], this unit is usually charged to only 50 to 60 keV. During pulsing, the voltage across the anode/cathode gap reaches a maximum value of approximately 85 keV, while the current reaches 10 to 15 kA [7].

SPARK GAP

A schematic of a low-impedance, triggered spark gap, the next element in an FX system, is shown in Fig. 8. The gap is charged to a voltage near self-breakdown; then, to initiate switching, a trigger pulse is fed in via the trigger electrode. This creates an over-voltage condition that initiates spontaneous breakdown. In some gaps, the trigger electrode is a concentric ring positioned midway between the anode and cathode elements as shown in Fig. 9. This particular gap is capable of carrying a current of 140 kA at a voltage of 120 keV. During operation, the gap is normally filled with SF_6 and argon. Nitrogen is used for lower voltage applications.

X-RAY TUBE

The output voltage pulse from the pulse-forming unit is carried to a vacuum diode. Two typical diodes are shown in Fig. 10. On the left-hand side is a transmission cathode diode used in low-voltage machines; on the right-hand side is a transmission anode diode used at high voltages. If the voltage pulse is negative, it is applied to the cathode; if positive, it is applied to the anode. At higher voltages, the anode and cathode are isolated from each other

by an insulator or a stack of insulators. Spacings between electrodes are set so that the negative surface begins to field-emit electrons. After a few ns, a plasma is formed, which will emit freely with low electric fields at the cathode.

The voltage/current relationship for diodes in planar geometry with circular cathodes and low magnetic fields can be described approximately by an equation originally developed by Langmuir [8] for vacuum tubes:

$$I = \frac{V^{3/2}}{k} \left(\frac{r^2}{d^2}\right), \tag{2}$$

where k is a constant, r is the cathode radius, and d is the electrode spacing. This expression applies only to diodes where magnetic fields are not important. At higher voltages and currents, the magnetic field of the beam tends to focus the electrons. Current for a planar diode under these conditions is given by

$$I_p = \frac{r}{d} I_A \gamma_0 \ln\left[\gamma_0 + \left(\gamma_0^2 - 1\right)^{1/2}\right], \tag{3}$$

where

$$\gamma_0 = \frac{eV + m_0c^2}{m_0c^2}. \tag{4}$$

In this expression, I_A is the Alfen current = 8.5 kA, V is the voltage across the diode, m_0 is the rest mass of the electron, c is the velocity of light, and I_p is the para-potential current [9].

In Eq. (3), consideration has been given to the effect of plasma motion, which leads to a time-dependent electrode spacing d.

Diode assemblies available commercially are as small as 10 cm in diameter for voltages under 100 keV and as much as a meter in diameter for units such as the 9-MeV machine previously described.

A cathode and three anodes from a transmission cathode diode are shown in Fig. 11. These anodes, used in FXD studies at LLL, have a conical 1.5-cm-long active region. Erosion of the anode under intense electron bombardment eventually makes it useless. The shorter anode shown has experienced about 20 pulses of 85-keV, 12-kA current.

The anode/cathode area of the 9-MeV machine discussed earlier is shown in Fig. 12. The actual x-ray active region is inside the 5-cm-diameter conical cathode structure. The function of these diodes is to convert the energy of the electrons into x-radiation through interaction with the anode.

The x-radiation useful in FXD, is produced by fluorescence. Beam electrons remove an electron from its shell in the atom, and an x-ray photon with a discrete energy is emitted as fluorescent radiation as a higher shell electron drops into that vacancy. Fluorescent radiation is isotropic and discrete. Most of the x-ray energy, however, especially in high voltage systems, is a result of the process of *bremsstrahlung*. A beam electron passes by a nucleus and is accelerated toward it; an x-ray photon is then emitted to conserve momentum and energy. This x-radiation will have a continuous spectrum from close to zero to near the total incident electron energy. The mean value of this spectrum occurs at 1/5 to 1/3 of the incident electron energy. At low voltages (<500 keV), the radiation will be essentially isotropic; at higher voltages, relativistic effects lead to a maximum in the forward direction. Calculated spectra for two diodes are shown in Fig. 13 [10]. Note the line radiation in the lower voltage diode shown in Fig. 13(a).

For a thick target, efficiency of conversion of electron energy into x-ray energy is given by

$$\varepsilon = \frac{(6 \times 10^{-4}\ ZV)}{(1 + 6 \times 10^{-4}\ ZV)} \quad , \tag{5}$$

where Z is the atomic number of the target and V is the electron energy in MeV [11]. With practical FXR sources in the 0.3- to 1.0-MeV range, we have measured efficiencies between 0.5 and 2.0% (somewhat lower than calculated by the above expression).

EVENT, TIMING

FX techniques can be used to study an exploding wire or foil, development of a jet by the action of a shaped charge, the behavior of a projectile as it moves through air or as it penetrates some material, shock-induced, microscopic transformations in materials, or any of a number of other high-speed phenomena. Specific examples of several of these and their study by FXR and/or FXD methods will be detailed shortly. Each event poses a timing problem which may be trivial or quite formidable. Sometimes it is sufficient to initiate the event and delay firing of the FX unit by a calculated amount using an electronic delay unit. Often it is necessary to arrange the start of this delay by sensing a prior event, such as the interruption of a light or x-ray beam [12] by the passage of a projectile. The timing problem for events requiring synchronization to 1 μs is trivial. Slightly greater levels of sophistication are needed to position events within an x-ray "window" which is between 1000 and 100 ns. Very sophisticated techniques are required below the 100-ns level. In such cases, it becomes necessary to sense the actual shock wave, determine (or if necessary, estimate) its velocity, and erect the high voltage pulse rapidly on the FX unit in time to coincide with the passage of the phenomena through the x-ray window. Few FXR applications require this level of sophistication, whereas many, if not most, of the more interesting FXD applications do.

DETECTORS

Detectors, like timing devices, range from the simple to the exotic. FX images often require enhancement, and this is the principal complication. Figure 14 shows three kinds of detectors using film: film without a screen, film with an intensifying screen, and film with image enhancement [13]. Scintillation detectors, arrays of detectors [14], or films with gated image enhancement [15] are less frequently used.

Since the event under study is often of a very destructive nature, it may also be necessary to provide elaborate safeguards so that the film or detection device is not destroyed. Figure 15 shows a blast cassette used in FXD studies [16]. Here, it was necessary to allow access to the film by the 8-keV X-rays and yet to deny access to blast products generated by the detonation of 150 g of a high explosive only 10 cm distant. The film and intensifying screen are indicated by G and F, respectively. These are contained in a light tight plastic bag D, protected from major abuse by foam cushions C and H and steel J, and shielded from small fragments by the slit assembly L-P.

FLASH X-RAY RADIOGRAPHY

In FXR, the object selectively absorbs some of the X-rays, and the remaining X-rays form a corresponding image. The intensity of the transmitted beam is given by

$$I = I_0 e^{-\mu t}, \tag{6}$$

where I_0 is the incident intensity, I is the transmitted intensity, μ is the absorption coefficient, and t is the path length. The absorption coefficient

is dependent on energy and material. X-rays are absorbed in three ways: through the photoelectric effect, through scattering, and through pair production. As x-ray photons collide with atoms of the absorbing material, they remove electrons and transfer energy to them. This is the *photoelectric effect*. It is an important process at low photon energies and is strongly dependent on atomic number. *Scattering* can be either coherent or incoherent. The former, resulting from the back-and-forth acceleration of an electron by the incident X-ray, is the process utilized in FXD. The latter, termed Compton scattering, occurs when an x-ray photon gives up part of its energy to an electron in the absorbing material and thereby has its trajectory modified. Scattering is dependent upon election density, and it slowly decreases with electron energy. *Pair production* occurs when an x-ray photon disintegrates in the vicinity of a nucleus to form an electron-positron pair. Approximately 1 MeV is required for this process, and the cross section increases with energy.

Absorption curves that consider these three effects are shown in Fig. 16 for three different elements. Data for these curves were obtained from Grosstein [17]. More extensive data are available in Plechaty, Cullen, and Howerton [18]. Three observations can be made from Fig. 16: (1) low-energy X-rays can be used very effectively to show differences in atomic number for materials; (2) absorption is relatively independent of energy above about 1 MeV and it shows a minimum of about 5 MeV depending on the atomic number of the absorber; high-intensity beams in this energy range are optimal for radiography of thick or dense objects; (3) photon energy above about 10 MeV may be counterproductive for higher-Z material because of increasing absorption due to pair production.

A practical FXR system has to take into account all of the previous considerations to provide sufficient x-ray flux at the target to expose the

detector and provide sufficient contrast to view the object. In fixed-pulselength Blumleins, some measure of flexibility with respect to exposure can be obtained by changing the dc charging voltage and the diode impedance.

Several FXR events are shown in Figs. 17-22 to illustrate some of the types of materials study possible and to point out some of the limitations. Most of these examples have been chosen to coincide with FXD analogues that will be discussed later. The macroscopic characterization of the event by FXR can thus be contrasted with the microscopic characterization by FXD.

An explosively produced shock wave is an obviously destructive phenomenon. Material experiencing the full effects of such an event comes apart as complex wave interactions lead to stresses exceeding tensile strengths. Figure 17 shows the breakup of a projectile fired from an explosively driven launcher [19] and traveling at a velocity slightly below 10 km/s. FXR radiographs permit a determination of the effect of changes in gun design and materials parameters. The changes are made to try to achieve projectile acceleration without breakup.

Figure 18 shows the successful launch of a projectile moving at the exceptional velocity of 12.2 km/s [20]. (To put this in perspective, we should note that the detonation velocity of the high-explosive PETN is only 8.3 km/s [21].) The projectile, fabricated from a lithium-magnesium material, is 0.66 cm in diameter and 0.36 cm long. Because of its velocity and the length (100 ns) of the FXR pulse, the radiograph is motion-blurred by over 1 mm.

The behavior of a material experiencing high dynamic stresses is shown in Fig. 19. This FXR photograph, taken with a 300-keV FX unit having a 20-ns pulse length, shows a penetrator which was traveling at 1 km/s, exiting from a target of mild steel [22]. Macroscopic motion of parts of the material can be inferred as the penetrator comes apart under tensile failure. The object

of such FXR studies is to tailor penetrator design and materials properties to avoid such failure.

Macroscopic changes in volume are readily observed by FXR, provided that there is a materials density contrast. Figure 20 shows a gas container in the process of being imploded by a high-explosive-driven liner of steel [20]. The collapsed region of the container can be seen easily in this photograph because of the density contrast between the compressed gas and the liner. An additional feature of interest here is the location of the detonation front. This photograph demonstrates one of the important features of FXR — its ability to probe the location of materials buried inside objects. (In this case, the steel liner and the compressed gas volume are contained within a high-explosive jacket.)

The object of this particular study was to determine implosion parameters so as to ensure that the gas was properly contained. Later, it was to be used to accelerate projectiles to hypervelocities. Too weak an implosion is bad, since the propellant gases will not ever be confined and compressed. Too vigorous an implosion is also bad, since the imploded liner will rebound and permit the gases to escape.

Another interesting event to study is a high-explosive-produced jet. If a high-explosive charge is shaped as an inverted cone and lined with metal, it will be capable of forming that liner into an extremely high velocity jet, very effective in drilling holes in materials. Unfortunately, the jet velocity is not constant. There is a high-velocity leading portion capable of penetration and a low-velocity tail that can plug the hole just drilled. Figure 21 shows a macroscopic FXR characterization of a jet [23]. The slower slug-forming portion is shown on the bottom half of this photograph. FXR studies of this nature permit tailoring of the shaped charge so as to eliminate the hole-plugging tail.

Time-dependent phenomena can be probed both by FXR and by FXD. Figure 22 shows the development of a crater as a function of time. The crater is being formed by explosion of a 3.5-cm-diameter sphere of C-4 explosive buried in plasticene clay [24]. The experimentally measured size and shape of this crater is used to normalize computer calculations of this phenomenon. Notice the increase, as a function of time, of the particle size of the crater debris. This series illustrates one of the special advantages of FXR over high-speed optical photography. The light from the explosion would prevent optical photography from recording details of the initial cratering. Examples of applications of FXR techniques to other interesting time-dependent phenomena, such as exploding wires, are shown in Jamet and Thomer [25].

FLASH X-RAY DIFFRACTION

The examples shown above of events studied by FXR and many more in the literature (see, for example, [25]), serve to point out that FXR techniques are suited to macroscopic characterization and that they are relatively mature in development. By contrast, FXD techniques, although dependent on much the same technology, are in the early stages of development and are particularly suited to microscopic characterization.

FXD is conventional x-ray diffraction conducted on a very short time scale. Making use of FXR hardware and techniques, FXD has opened a radically new region of materials study. Figure 23 shows qualitatively the regions of pressure/time space reachable by means of conventional versus flash x-ray diffraction. The upper limit of static-pressure x-ray measurement is around 50 GPa [26], although recent experiments suggest that 100 GPa may soon be attainable [27]. Such experiments require extremely long exposures, however, lasting in some cases a week or more. FXD is well suited to events occurring

in times less than 1 μs but more than 1 ns. Perhaps 50- to 200-ns events are optimal at present. By taking advantage of the very high pressures attainable via shock waves, we should some day be able to use FXD to study materials at 100 GPa and beyond. The current upper limit is below 50 GPa.

Several historical reviews of FXD have been written [25,28]. Currently, FXD work is carried out in only a handful of laboratories, of which LLL has been one of the most active. Much of the work we will describe was done at LLL.

To conduct a diffraction experiment in the very short time periods described, it is necessary to replace conventional dc sources with flash units having very much higher instantaneous brilliancy factors. Two approaches have been used. In one of these, conventional FXR units were adapted to diffraction requirements [28]. There is a problem in this approach, however. FXD requires low-voltage, high-current systems, whereas FXR usually stresses voltage at the expense of current. The necessary compromises result in very weak images and high backgrounds. A more successful approach pursued at LLL has been to adapt a research FXR unit especially built for radiographic studies requiring a high-current, low-voltage source. This device, already described in Fig. 7, has characteristics similar to those needed for FXD, i.e., a small focal spot, moderate voltage, high current, a short and easily modified pulse length, and a short (<1/2 μs) interval between trigger pulse and x-ray pulse. Focal spot diameter is ~2 mm and x-ray intensity is moderately reproducible. By contrast, the focal spot of the 9-MeV FXR unit has been described as between 3 and 10 mm, depending upon x-ray energy.

A series of pinhole photographs of the LLL FXD anode is shown in Fig. 24. An interesting but bothersome phenomenon is observed on the second photograph. The tip of the conical anode has a "blossom" appearance due to the fracturing of the tip by the impact of the intense electron bombardment

on the first fire. This feature disappears in subsequent fires as the material erodes. The fifth fire is particularly weak as a result of premature switching in the triggering circuits.

As mentioned earlier, the instantaneous brilliancy of such devices surpasses that of standard dc microfocus units by several orders of magnitude. It even surpasses state-of-the-art rotating anode machines by 2 or 3 orders of magnitude. An approximate comparison is shown in Fig. 25. In spite of this advantage, it is found that compromises must be made to carry out diffraction investigations with FX units. One quick remedy is to place the material close to the source, sacrificing resolution for intensity. Typical, sample-to-source distances are ~10 to 12 cm and equivalent sample-to-film distances as required. A schematic of a conventional FXD experiment is shown in Fig. 26. With the arrangement shown, it is possible to obtain diffraction records of the quality shown in Fig. 27. Both records were made using a single pulse of copper radiation on a LiF sample. The upper one shows a portion of the powder pattern obtained from a polycrystalline sample, and the lower one shows diffraction from the 200 reflection of a single crystal of LiF. The discontinuity in the image resulted from a lead foil mask placed over the center of the crystal for alignment purposes.

An actual FXD experiment using a high explosive to study the effect of high dynamic pressure on a crystalline material is shown in Fig. 28. At the bottom of this photograph is the armor plate used to protect the anode area of the x-ray machine from damage due to the high-velocity fragments produced by the shock-wave generator. The generator, consisting of a detonator, a shaped charge, and a high-explosive booster, is shown in the central part of this photograph. It is supported by an inexpensively fabricated goniometer device, which permits orientation of the sample at the correct Bragg angle with respect to the source, and of the camera, shown at the top of the

photograph, with respect to the sample. The camera is an assembled version of that shown in Fig. 15. Protruding from the front of the sample holder are shock-wave probes used to sense the location of the shock wave and to obtain its velocity. The x-ray source is triggered by a pulse from one of these probes.

This apparatus has been used to answer a variety of questions. Perhaps the simplest and certainly the most fundamental concerns order. Is there crystalline order behind the shock front, or is there rather a state of frenzied atomic motion and chaotic confusion of atoms? Underlying this question is the concern that the obviously violent and destructive nature of the shock-wave process might be inimical to crystalline order. It is conceptually difficult, upon first consideration, to imagine how the process can do more than disorganize the crystal lattice into a nearly amorphous entity. As the FXR study of projectile breakup illustrates, disintegration is possible on the macroscopic scale.

The answer to this important question came out of FXD studies on polycrystalline materials. It was shown that it is possible to obtain a diffraction record from a shock-compressed polycrystalline sample. An example of these results is shown in Figure 29 [29]. The top record, obtained before shock-wave compression, shows the first two diffraction lines of the powder pattern of LiF. The bottom record shows the pattern obtained during shock-wave compression to approximately 18 GPa. This record tells us that not only is the material behind the shockfront ordered, it is actually experiencing approximately *hydrostatic* pressure conditions. This follows from a measurement of the $\Delta 2\theta$ shift of the powder lines, which indicate directly how much the atoms have moved as a result of the shock pressure.

These results led to a study of the behavior of single crystals under shock-wave compression. The object was to shed some light on the question of atomic motion. Exactly how is it possible for apparently hydrostatic conditions to be obtained at the atomic level, when the sense of the shock-wave is unidirectional? We contrast this study to the FXR study of the penetrator, which implied macroscopic motion transverse to the initial penetrator velocity vector.

Results from two different single-crystal materials are shown in Fig. 29(b)[30]. The top record was obtained from a single crystal of LiF shock-compressed to about 30 GPa. Features from left to right are $K_\beta 200$ and $K_{\alpha} 200$ from the uncompressed lattice, and $K_\alpha 200$ from the shock-compressed LiF. The bottom record shows diffraction from the 002 reflection of pyrolytic graphite shock-compressed to about 20 GPa. From considerations of the intensity of the diffracted reflection obtained from the shock-affected portion of the crystal, it can be deduced that the crystal does not disintegrate into a lot of randomly oriented crystallites, but rather, to a first approximation, behaves as though it is still a single crystal with orientation unchanged. The results of these experiments suggest that models of microscopic motion behind the shock-front must preserve crystal order and orientation, while accounting for motion transverse to the shock vector to effect the hydrostatic condition demonstrated by the earlier polycrystalline experiments.

FXR studies of volume changes have an analogue in the powder and single crystal FXD studies. In addition, it will now be shown how FXD can help to characterize materials undergoing discontinuous volume changes.

A pivotal question in shock-wave studies concerns phase transformations behind the shock front. Bancroft, Peterson, and Minshall's study of shock-compressed iron [31] using conventional shock-wave techniques led to the

conclusion that phase transformations could occur in the very short time intervals involved in a shock-wave experiment. Unfortunately, such measurements are indirect and do not establish that the phase transformation hypothesis is the unique and correct description of the observed phenomena. X-ray diffraction offers a direct test. Upon transformation to a different structure, the diffraction pattern changes so that, were it possible to observe the pattern from material presumably undergoing a transformation behind a shock wave, it should be clear that a new crystalline modification had formed.

In FXD studies conducted with BN, Johnson and Mitchell [32] showed that it is possible to say conclusively that a phase transformation has occurred, to say what the new structure is, and to establish a mechanism for the transformation. The records obtained in that study are shown in Fig. 30. The top record, taken before the shock compression, shows a partial pattern of the graphite-like normal low-pressure structure. The bottom record was taken as the sample was experiencing a shock pressure of about 25 GPa. The new features in this record establish that the material has transformed to the Wurtzite (diamond-like) structure. This type of study holds promise of answering many interesting questions on shock-induced pressure transformations.

A diffraction technique only partially exploited in FXD studies to date is that of Laue photography. Figure 31(a) shows the geometry for a transmission Laue experiment. The results obtained from a single pulse of 40-μs Mo X-rays onto a thin sample of copper are shown in Fig. 31(b). This is a very weak image, and it would probably require enhancement if this particular material were used in an experiment under dynamic conditions. Considerably better results were obtained by Jamet [33] using this method on a single crystal of aluminum exploded by a capacitor discharge.

One of the weaknesses of the high-explosive method of shock generation in connection with the FXD studies is that only small quantities of explosives can be used if the film record is to be preserved. This means that simultaneous diffraction and shock-velocity measurements are difficult to obtain with great accuracy. One way around this problem is to do the separate measurements on separate but equivalent samples. A better way would be to devise a method for carrying out the diffraction experiment on a gas gun, where a precise determination of pressure is possible and where higher pressures can be obtained. Research in Japan is proceeding in this direction [34].

In independent experiments, Green [35] and Jamet and Thomer [36] have attempted to characterize the crystallite size of material comprising an explosively driven jet. Figure 32 shows the experimental arrangement employed by Jamet and Thomer as well as their results. A shaped charged, confined in a blast container, produces a jet of aluminum. This jet contacts the foil and turns on the x-ray unit in time to obtain a diffraction powder pattern of the polycrystalline aluminum in the jet. The studies of Green show that the jet was composed of particles between 0.01 and 1.0 mm in size. The results of Jamet and Thomer, indicate a smaller average crystallite size. The left-hand photograph was taken before the jet was formed, and the right-hand photograph was taken 5 μs after initiation of the shaped charge. These studies clearly complement the earlier described macroscopic characterization of jets.

The time-dependent process encountered in the explosion of a gold foil by a capacitor discharge has been studied by Jamet [37]. The transmission powder pattern taken with copper K_α radiation are shown in Fig. 33. The upper left picture shows the foil at rest; the upper right picture was taken 1.3 μs after the beginning of the capacitor discharge; the lower left and

right pictures were taken at 1.5 and 1.8 μs, respectively. The vanishing of the diffraction pattern 1.8 μs after the discharge gives evidence that the vapor state has been reached.

One of the foremost problems encountered in FXD is that of synchronizing the x-ray pulse to the event of interest. In some of the foregoing experiments, this was not a major concern because the event had a reasonably long lifetime. Both the jet and exploding foil experiments fall into this category. The studies of the response of crystalline material to shock waves, however, require much more accurate timing. Some of these events last 10 ns or less.

Methods to increase event lifetimes are thus of obvious interest. Egorov, Nitochkina, and Orekin [38] increased the lifetime of the shock-compressed state of aluminum by sandwiching a semi-transparent anvil of lithium over it. This greatly extends the time period over which it is possible to view the shock-compressed state, but it has an undesirable drawback. Due to the impedance mismatch between the sample and the anvil, the pressure drops considerably as soon as the shock wave reaches the sample/anvil interface. Nevertheless, a shock pressure of 14 GPa was attained.

The wedge method of Johnson, Mitchell, and Evans [39] is one way of increasing the event lifetime without producing the problem described above. A wedge-shaped base under the sample causes the shock wave to enter the sample at an angle. As a result, different parts of the sample are at different states, and a slit-shaped beam of X-rays can then probe the sample before, during, and after compression to give a time history of the event on a single record.

SUMMARY

The examples given here of the use of FXR and FXD in materials testing show the wide variety of problems that may be tackled. By contrasting FXR examples with approximately equivalent FXD examples, some appreciation of the types of questions each technique addresses has been obtained . These are complementary techniques; FXR is a tool for macroscopic characterization of materials, and FXD is a tool for microscopic characterization. Together, they permit access to a unique domain of NDT by virtue of the extremely short pulse lengths available from field-emitting flash x-ray devices.

ACKNOWLEDGMENTS

We wish to thank A. Mitchell, L. Evans, J. Scudder, M. Van Thiel, K. Seifert, and F. Jamet for providing some of the material used in this manuscript. The spectrum in Figure 13(a) was calculated by S. Gair of Sandia Livermore Laboratory and used by permission. This work was partially supported by the U. S. Energy Research and Development Administration.

REFERENCES

1. Turner, R. E., "Big Shot," INDUSTRIAL RES., (August 1976) 43-45.

2. Marx, E., "Versuche uber die Prufung von Isolatoren mit Spannungsstossen," ELEKTROTECHNISCHE ZEITSCHRIFT, 45 (1925), 652.

3. Bernstein, B. and Smith, I., "Aurora, an Electron Accelerator," I.E.E.E. TRANS. NUCL. SCI. NS-20, no. 3 (1973), 294-300.

4. Champney, P. D'A., and Spence, P., "PULSERAD 1480 — A 9 MV Pulsed Electron Accelerator with Intensely Focused Beam," I.E.E.E. TRANS. NUCL. SCI., NS-22, no. 3 (1975), 970-974.

5. Martin, J. C. "Nanosecond Pulse Techniques," United Kingdom Atomic Energy Association, Berkshire, Rept. SSWA/JCM/704/49, (1970).

6. Motz, J. W., Dick C. E., Lucas, A. C., Pacious, R. C., and Sparrow, J. H., "Production of High Intensity K X-ray Beams," J. APPL. PHYS., 42, no. 5 (1971), 2131-2133.

7. Pellinen, D. G., Johnson, Q., and Mitchell, A., "A Picosecond Risetime High Voltage Divider," REV. SCI. INST. 45, no. 7 (1974), 944-946.

8. Langmuir, I. and Compton, K. T., "Electrical Discharges in Gases, Part II. Fundamental Phenomena in Electrical Discharges," REV. MOD. PHYS., 3, no. 2 (1931), 191-257.

9. Creedon, J. M., "Relativistic Brillouin Flow in the High ν/γ Diode," J. APPL. PHYS., 46, no 7 (1975), 2936-2955.

10. Personal communications, S. Gair, 1974.

11. Koch, H. W., and Motz, J. W., "Bremsstrahlung Cross-Section Formulas and Related Data," REV. MOD. PHYS., 31, no. 4 (1959), 920-955.

12. Long, J. R., and Mitchell, A. C., "A dc X-Ray Fiducial Pulse Generator for Light-Gas Gun Work," REV. SCI. INST., 43, no. 6 (1972), 914-916.

13. Green, R. E., Jr., "Electro-Optical Systems for Dynamic Display of X-Ray Diffraction Images," in ADVANCES IN X-RAY ANALYSIS, Vol. 14, Proceedings of the 19th Annual Conf. on Applications of X-Ray Analysis, Denver, Aug. 5-7, 1970, ed. by C. S. Barrett, J. B. Newkirk, and C. O. Rund, New York: Plenum Press (1971), 311-337.

14. Johnson, Q., Mitchell, A., and Evans, L., "X-Ray Detector for Dynamic Diffraction Studies," REV. SCI. INST., 42, no. 7 (1971), 999-1001.

15. Kusa, G. W. and Chang, J. "Nanosecond Time Resolved X-Ray Diagnostics of Relativistic Electron Beam Initiated Events," in ADVANCES IN X-RAY ANALYSIS, Vol. 18, Proceedings of the 23rd Annual Conf. on Application of X-Ray Analysis, Denver, Aug. 7-9, 1974, ed. by W. L. Pickles, C. S. Barrett, J. B. Newkirk, and C. O. Ruud, New York: Plenum Press (1975), 107-116.

16. Mitchell, A. C., Johnson, Q., and Evans, L., "A Film System for Flash X-ray Diffraction Studies of Shock-Compressed Materials," REV. SCI. INST., 44, no. 5 (1973), 597-599.

17. Grosstein, G. W., "X-ray Attenuation Coefficients from 10 kV to 100 MV," National Bureau of Standards, Report 583 (1957).

18. Plechaty, E. F., Cullen, D. E., and Howerton, R. J., "Tables and Graphs of Photon Interaction Cross Sections from 1 kV to 100 MV," Lawrence Livermore Laboratory, Livermore, California Report UCRL-50400, Vol. 6, Rev. 1 (1975).

19. Seifert, K. and Crispino, A., "Feasibility Study of Explosively Driven Hypervelocity Projectiles," Physics International Company, San Leandro, California, Report PIFR-559 (1974).

20. "Testing of Large Shaped Charges," Physics International Company, San Leandro, California, Report PIP-1140B (1972).

21. Dobratz, B. M., "Properties of Chemical Explosives and Explosive Stimulants," Lawrence Livermore Laboratory, Livermore, California, Report UCRL-51319, (1972), 8-1.

22. Personal communication, J. Scudder, 1976.

23. Van Thiel, M., Wilkins, M., and Mitchell, A., "Shaped Charge Sequencing," INT. J. ROCK MECH. MIN. SCI. & GEOMECH. ABSTS., 12, no. 9, (1975) 283-288.

24. Seifert, K. and Maxwell, D., "Experimental Interim Report of Cratering Displacement Ejecta Processes," Physics International Company, San Leandro, California, Report PITR-659-1 (1974).

25. Jamet, F. and Thomer, G., FLASH RADIOGRAPHY. New York: American Elsevier Publishing Co., Inc. (1976).

26. Personal communication, G. Piermarmi, 1976.

27. Mao, H. K., and Bell, P. M., "High Pressure Physics: The 1 Mbar Mark on the Ruby R_1 Static Pressure Scale," SCIENCE, 191, no. 4229 (1976), 851-852.

28. Carbonnier, F. M., "Proposed Flash X-ray System for X-ray Diffraction with Submicrosecond Exposure Time," in ADVANCES IN X-RAY ANALYSIS, Vol. 15, Proceedings of the 20th Annual Conf. on Applications of X-ray Analysis, Denver, August 11-13, 1971, ed. by K. F. J. Heinrich, C. S. Barrett, J. B. Newkirk, and C. O. Rudd. New York: Plenum Press (1972), 446-461.

29. Johnson, Q., Mitchell, A., and Evans, L., "X-ray Diffraction Evidence for Crystalline Order and Isotropic Compression During the Shock-Wave Process," NATURE, 231, no. 5301 (1971), 310-311.

30. Johnson, Q., Mitchell, A., and Evans, L., "X-ray Diffraction Study of Single Crystals Undergoing Shock-Wave Compression," APPL. PHYS. LETT., 21, no. 1 (1972), 29-30.

31. Bancroft, D., Peterson, E. L., and Minshall, S., "Polymorphism of Iron at High Pressure," J. APPL. PHYS., 27, no. 3 (1956), 291-298.

32. Johnson, Q. and Mitchell, A., "First X-ray Diffraction Evidence for a Phase Transition During Shock-Wave Compression," PHYS. REV. LETT. 29, no. 20 (1972), 1369-1371.

33. Jamet, F., "Diagramme de Laue en Radiographic Instantanée," C. R. ACAD. SCI., Ser. B, 271, no. 14 (1970), 714-717.

34. Kondo, K., Sawaoka, A., and Saito, S., "A Trial Construction of the Flash X-ray Diffraction System for Shock Wave Studies," PROC. 4TH INT. CONF. ON HIGH PRESSURE, Kyoto 1974 [The Physico Chemical Society of Japan, Kyoto (1975)], 845-851.

35. Green, R. E., Jr., "First X-ray Diffraction Photograph of a Shaped Charge Jet," REV. SCI. INST., 46, no. 7 (1975), 1257-1261.

36. Jamet, F., and Thomer, G., "Diagramme de Poudre d'un Jet de Charge Creuse," C. R. ACAD. SCI., Ser. B, 279, no. 19 (1974), 501-503.

37. Jamet, F., "Recording of X-ray Diffraction Patterns Using Flash X-rays in Connection with an Image Intensifier," J. SMPTE, 80, no. 11 (1971), 900-901.

38. Egorov, L. A., Nitochkina, E. V., Orekin, Yu. K., "Registration of Debyegram of Aluminum Compressed by a Shock Wave," JETP LETT., 16, no. 1 (1972), 4-6.

39. Johnson, Q., Mitchell, A., and Evans, L., "Time-Resolved X-ray Diffraction Study of Crystals Undergoing Shock-Wave Compression," to be published.

FIGURE CAPTIONS

Fig. 1. Time requirements for various x-ray experiments. The dashed line indicates the approximate boundary between exposures requiring continuous sources and exposures requiring pulsed sources. A radiograph of the Liberty Bell required 7.5 hours [1].

Fig. 2. Seven elements of a flash x-ray experiment.

Fig. 3. Simple flash x-ray unit consisting of a voltage source, charging resistor R, storage capacitor C, and flash tube T. Addition of lower-left circuit element containing a triggerable spark gap G, permits timing. Insertion of lower right element containing a pulse transformer Tr, permits pulse shaping.

Fig. 4. Schematic of Marx generator.

Fig. 5. Marx generator room of the 9-MeV flash radiographic unit. Vertically stacked capacitors are interconnected by spark gaps and isolation resistors, consisting of solutions of $CuSO_4$ in plastic tubes.

Fig. 6. The 9-MeV, 200-kA, 75-ns flash x-ray unit for radiographic studies.

Fig. 7. Schematic of low-voltage, high-current FXD device.

Fig. 8. Schematic of triggerable spark gap.

Fig. 9. Triggerable spark gap. Trigger electrode is the cylindrical device at midplane in the gap.

Fig. 10. Flash x-ray diodes.

Fig. 11. Anodes (lower left) and cathode (upper right) from a demountable flash x-ray diode used for diffraction.

Fig. 12. Anode/cathode area of 9-MeV flash x-ray unit.

Fig. 13. Calculated x-ray spectra for two flash x-ray diodes.

Fig. 14. Three basic methods of detection used in FX.

Fig. 15. Blast cassette used in FXD studies.

Fig. 16. Absorption coefficient for C, Fe, and Pb versus x-ray photon energy.

Fig. 17. Flash radiographs of projectile breakup.

Fig. 18. Flash radiograph of lithium-magnesium projectile flying in air at 12.2 km/s. Fiducial mark is 1.27 cm.

Fig. 19. Heavy rod penetrator undergoing tensile fracture upon exit from a steel target.

Fig. 20. Collapse of a conical gun barrel imploded by a high explosive.

Fig. 21. Jet formed by a shaped charge. The bottom half of the photograph is a continuation of the top half. The jet is traveling from right to left.

Fig. 22. Flash radiographs of cratering by an explosive sphere half buried in plasticene clay. Pictures were taken at 50, 200, 500, and 3000 μs after detonation.

Fig. 23. Pressure/time domain for conventional and flash x-ray diffraction experiments.

Fig. 24. Pinhole photographs of ten consecutive fires from a FXD source.

Fig. 25. Source brilliancy for continuous x-ray sources and the FXD source used at LLL.

Fig. 26. Geometry of FXD experiment.

Fig. 27. FXD photographs taken of LiF using a Cu anode. Upper record is from a polycrystalline sample, lower one is from a single crystal.

Fig. 28. Actual experimental configuration of a FXD experiment.

Fig. 29. FXD records from shock-wave experiments:

a) Obtained from polycrystalline LiF; top image is before shock compression; lower is during shock compression.

b) Obtained from single crystal undergoing shock wave compression; the top record is from a LiF crystal; the bottom record is from a graphite crystal.

Fig. 30. FXD records of the phase transformation in BN.

Fig. 31. a) Schematic for FXD transmission Laue photograph;

b) Laue photograph of thin copper foil using a Mo anode FXD unit.

Fig. 32. FXD experiment of an explosively-produced jet:

a) Schematic of experiment;

b) Powder pattern before (left) and during (right).

Fig. 33. Transmission powder patterns of an exploding gold foil.

KM/edas/ms/1mc

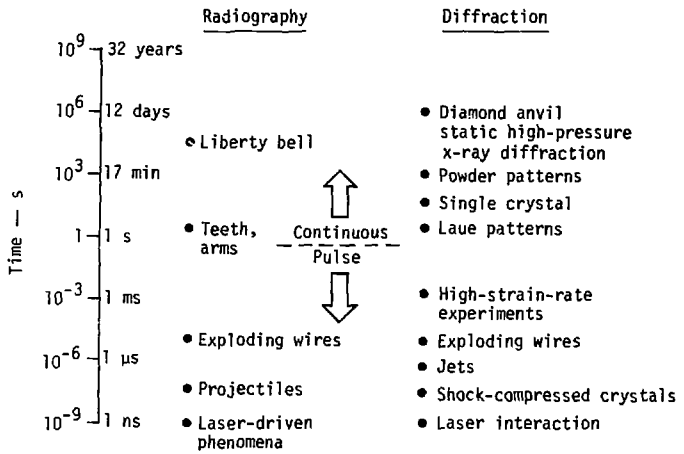

Fig. 1. Time requirements for various x-ray experiments. The dashed line indicates the approximate boundary between exposures requiring continuous sources and exposures requiring pulsed sources. A radiograph of the Liberty Bell required 7.5 hours [1].

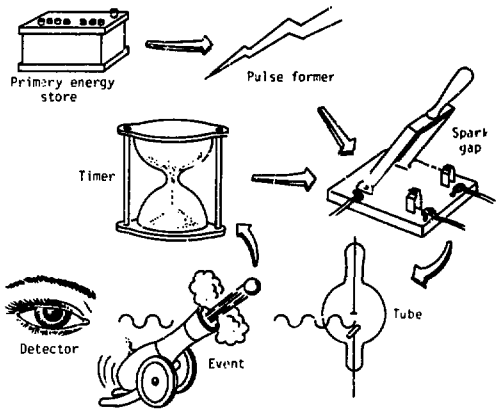

Fig. 2. Seven elements of a flash x-ray experiment.

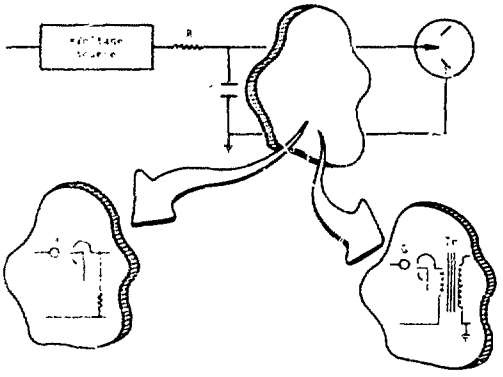

Fig. 3. Simple flash x-ray unit consisting of a voltage source, charging resistor R, storage capacitor C, and flash tube T. Addition of lower-left circuit element containing a triggerable spark gap G, permits timing. Insertion of lower right element containing a pulse transformer Tr, permits pulse shaping.

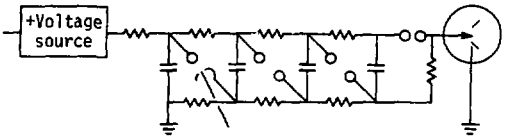

Fig. 4. Schematic of Marx generator.

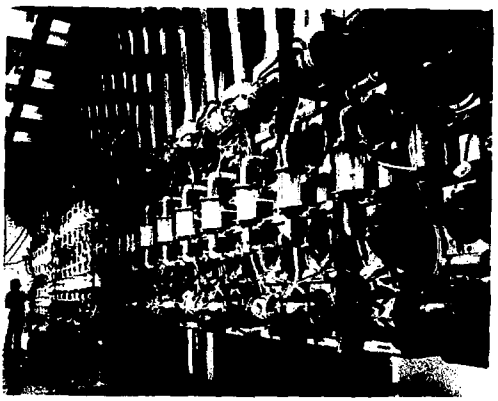

Fig. 5. Marx generator room of the 9-MeV flash radiographic unit. Vertically stacked capacitors are interconnected by spark gaps and isolation resistors, consisting of solutions of $CuSO_4$ in plastic tubes.

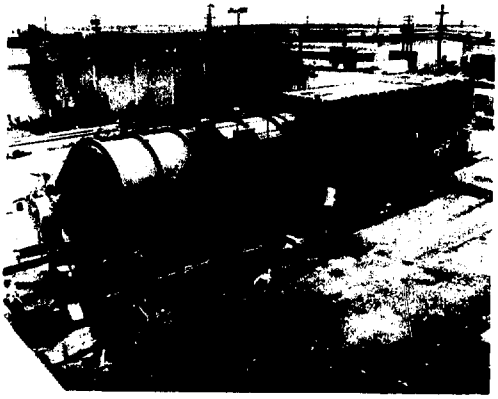

Fig. 6. The 9-MeV, 200-kA, 75-ns flash x-ray unit for radiographic studies.

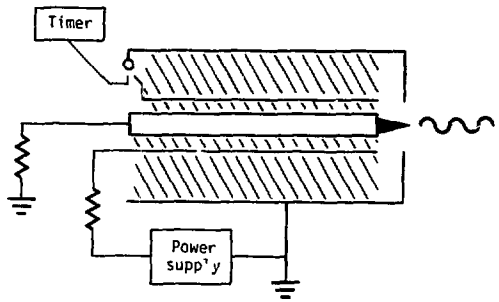

Fig. 7. Schematic of low-voltage, high-current FXD device.

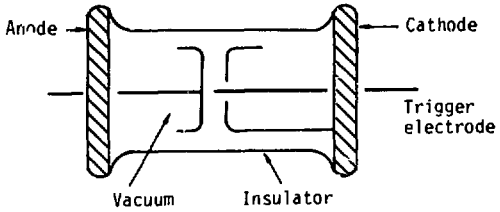

Fig. 8. Schematic of triggerable spark gap.

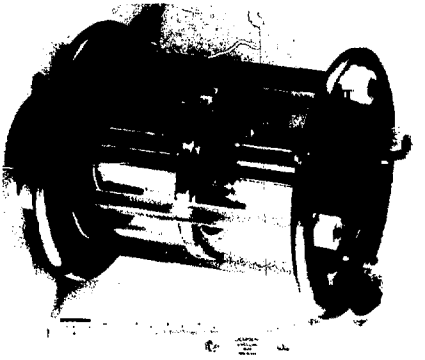

Fig. 9. Triggerable spark gap. Trigger electrode is the cylindrical device at midplane in the gap

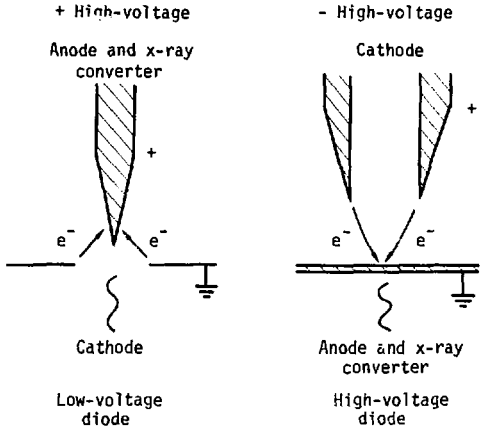

Fig. 10. Flash x-ray diodes.

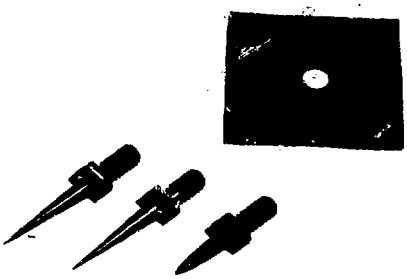

Fig. 11. Anodes (lower left) and cathode (upper right) from a demountable flash x-ray diode used for diffraction.

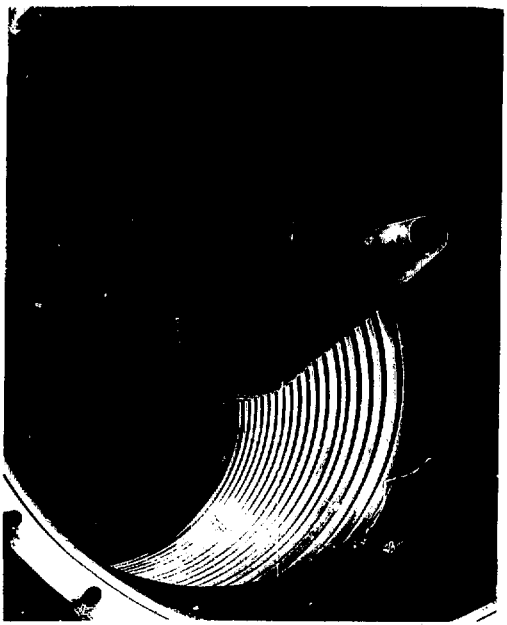

Fig. 12. Anode/cathode area of 9-MeV flash x-ray unit.

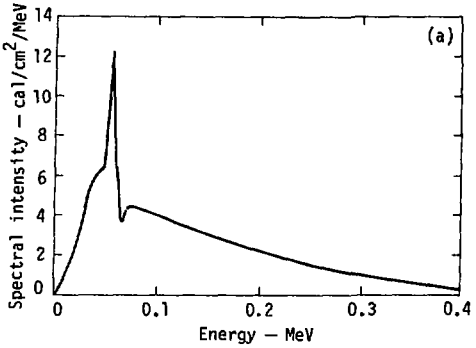

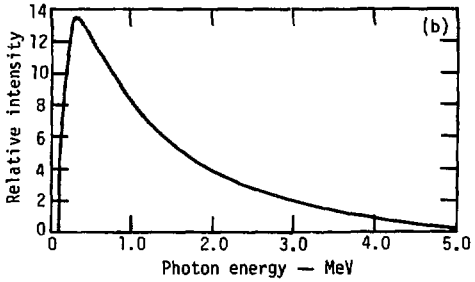

Fig. 13. Calculated x-ray spectra for two flash x-ray diodes.

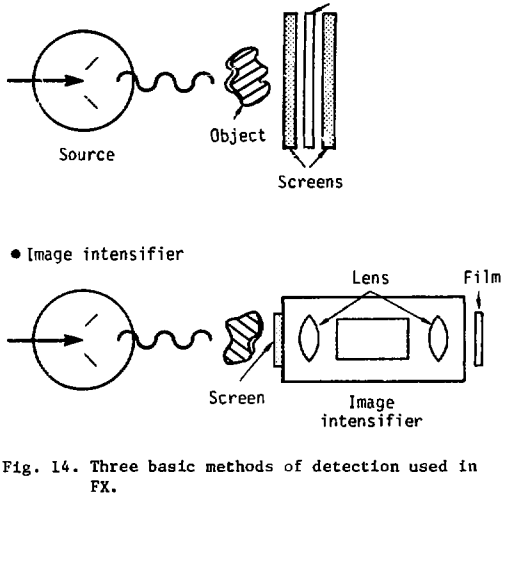

Fig. 14. Three basic methods of detection used in FX.

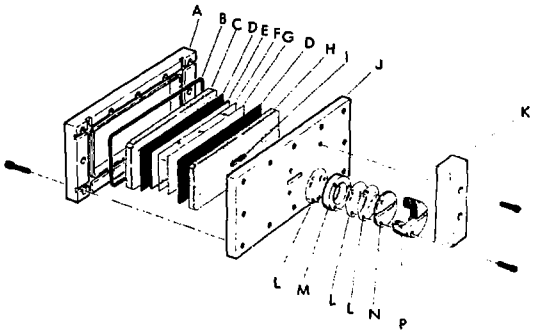

Fig. 15. Blast cassette used in FXD studies.

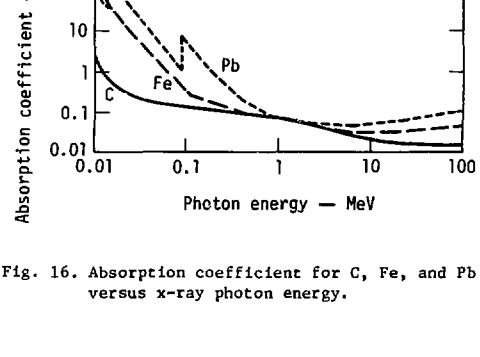

Fig. 16. Absorption coefficient for C, Fe, and Pb versus x-ray photon energy.

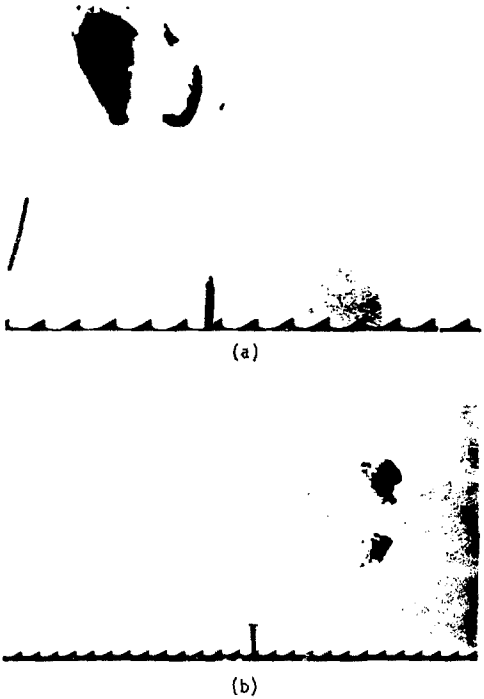

Fig. 17. Flash radiographs of projectile breakup.

Fig. 18. Flash radiograph of lithium-magnesium projectile flying in air at 12.2 km/s. Fiducial mark is 1.27 cm.

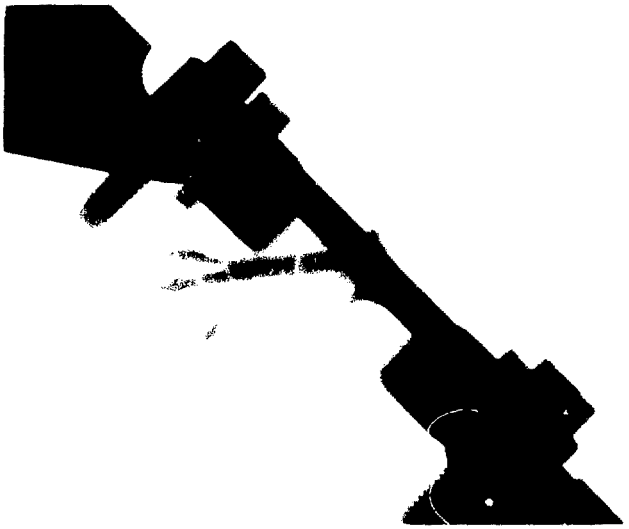

Fig. 19. Heavy rod penetrator undergoing tensile fracture upon exit from a steel target.

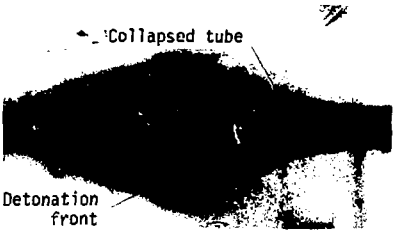

Fig. 20. Collapse of a conical gun barrel imploded by a high explosive.

Fig. 21. Jet formed by a shaped charge. The bottom half of the photograph is a continuation of the top half. The jet is traveling from right to left.

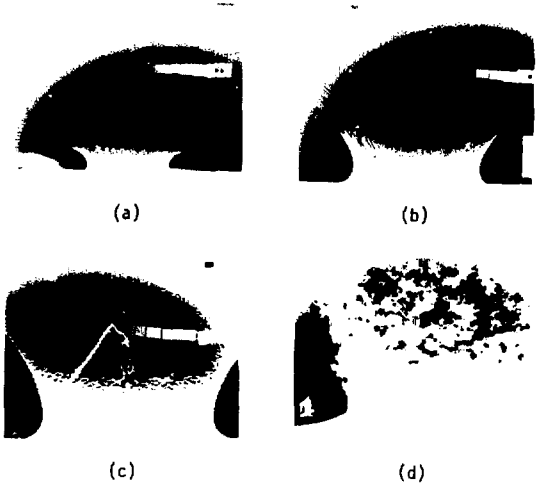

Fig. 22. Flash radiographs of cratering by an explosive sphere half buried in plasticene clay. Pictures were taken at 50, 200, 500, and 3000 μs after detonation.

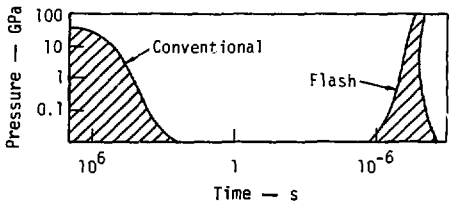

Fig. 23. Pressure/time domain for conventional and flash x-ray diffraction experiments.

Fig. 24. Pinhole photographs of ten consecutive fires from a FXD source.

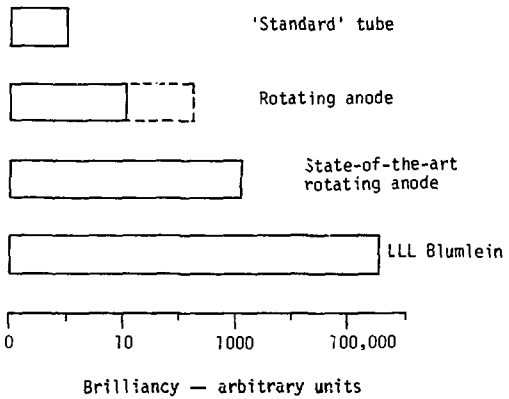

Fig. 25. Source brilliancy for continuous x-ray sources and the FXD source used at LLL.

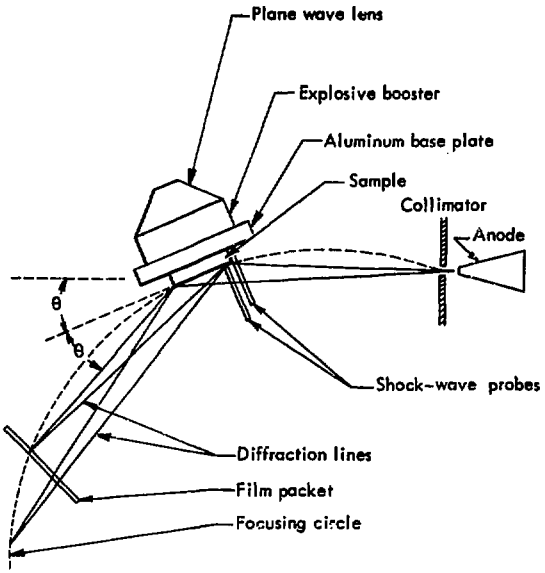

Fig. 26. Geometry of FXD experiment.

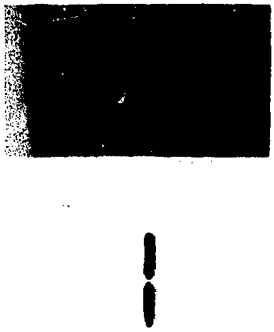

Fig. 27. FXD photographs taken of LiF using a Cu anode. Upper record is from a polycrystalline sample, lower one is from a single crystal.

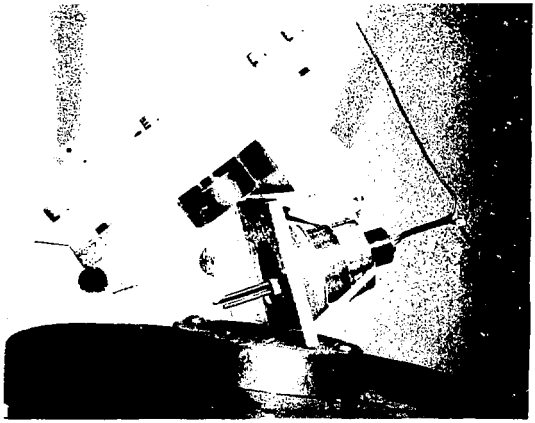

Fig. 28. Actual experimental configuration of a FXD experiment.

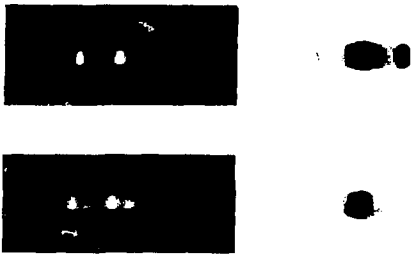

(a) (b)

Fig. 29. FXD records from shock-wave experiments:
a) Obtained from polycrystalline LiF; top image is before shock compression; lower is during shock compression.
b) Obtained from single crystal undergoing shock wave compression; the top record is from a LiF crystal; the bottom record is from a graphite crystal.

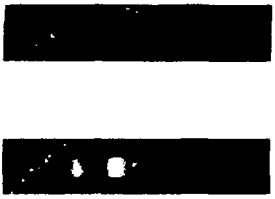

Fig. 30. FXD records of the phase transformation in BN.

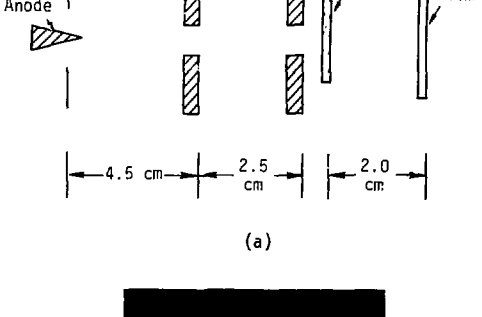

(a)

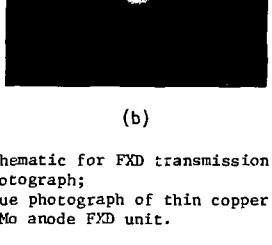

(b)

Fig. 31. a) Schematic for FXD transmission Laue photograph;
b) Laue photograph of thin copper foil using a Mo anode FXD unit.

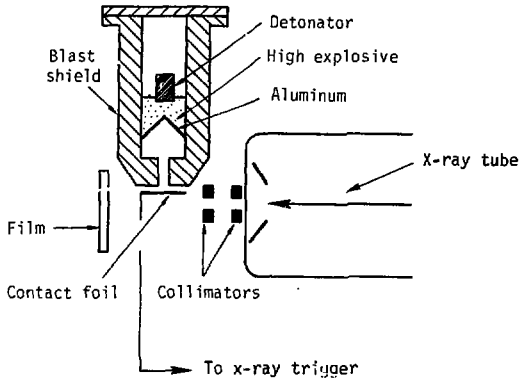

(a)

(b)

Fig. 32. FXD experiment of an explosively-produced jet:
a) Schematic of experiment;
b) Powder pattern before (left) and during (right).

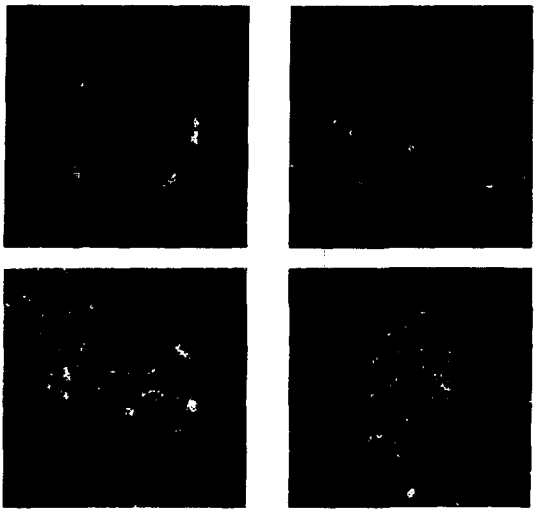

Fig. 33. Transmission powder patterns of an exploding gold foil.